

3D FACIAL IMPERFECTION REGENERATION: DEEP LEARNING APPROACH AND 3D PRINTING PROTOTYPES

Phuong D. Nguyen^{1,*}, Thinh D. Le^{1,*}, Duong Q. Nguyen², Thanh Q. Nguyen¹, Li-Wei Chou³, H. Nguyen-Xuan^{1,4,†}

¹CIRTECH Institute, HUTECH University, Ho Chi Minh City, Viet Nam

²Department of Mathematics and Statistics, Quy Nhon University, Quy Nhon City, Viet Nam

³Department of Physical Medicine and Rehabilitation, China Medical University Hospital, Taichung, Taiwan

⁴Department of Medical Research, China Medical University Hospital, China Medical University, Taichung, Taiwan

ABSTRACT

This study explores the potential of a fully convolutional mesh autoencoder model for regenerating 3D nature faces with the presence of imperfect areas. We utilize deep learning approaches in graph processing and analysis to investigate the capabilities model in recreating a filling part for facial scars. Our approach in dataset creation is able to generate a facial scar rationally in a virtual space that corresponds to the unique circumstances. Especially, we propose a new method which is named 3D Facial Imperfection Regeneration(3D-FaIR) for reproducing a complete face reconstruction based on the remaining features of the patient face. To further enhance the applicable capacity of the present research, we develop an improved outlier technique to separate the wounds of patients and provide appropriate wound cover models. Also, a Cir3D-FaIR dataset of imperfect faces and open codes was released at <https://github.com/SIMOGrouP/3DFaIR>. Our findings demonstrate the potential of the proposed approach to help patients recover more quickly and safely through convenient techniques. We hope that this research can contribute to the development of new products and innovative solutions for facial scar regeneration.

Keywords Fully convolutional mesh autoencoder · 3D object regeneration · imperfect face · deep learning · graph processing · facial scar restoration

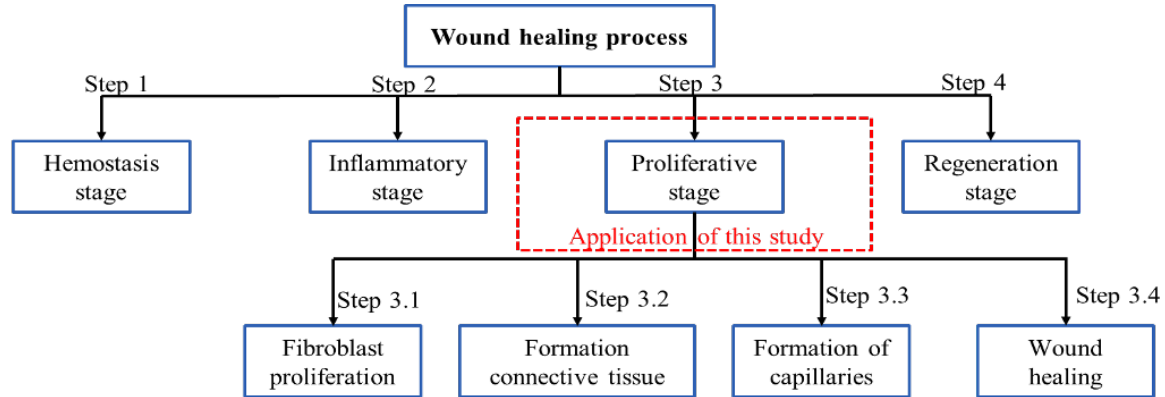
1 Introduction

The field of reconstructing physical flaws in the human body plays significant importance due to its widespread relevance to daily life. Physical disabilities are frequently caused by various factors such as job accidents, traffic accidents, and wars. The presence of disability in the body patient can cause numerous challenges in life, both physically and mentally. One such manifestation is the formation of scars, which are the marks left behind following the healing process of external injuries due to trauma. Except for minor traumas, all wounds originating from accidents, infections, or surgery often produce scars. When the skin is wounded, its recovery and regeneration should meet four stages, including the hemostasis stage, inflammatory stage, proliferative stage, and regeneration stage, as depicted in Fig. 1. The shape of the scar and how to treat scars are determined by a variety of factors, including the depth, size, and location of the wound as well as the age, sex, and genetics of each patient. Among the steps, step 3 is almost the most important one, which consists of fibroblast proliferation, formation of connective tissue, formation of capillaries, and wound healing. The patient care method must be very attentive throughout this period in order for the wound to heal spontaneously. In accordance with the request of the treating doctor, wounds must be cleaned and disinfected on a regular basis. When the wound dressing process is ineffective, the dressing process may be tough, and it may not be safe to clean the wound. Such an issue becomes problematic and has not been entirely resolved. Scars are unattractive and may lead to physical and emotional symptoms such as itching, pain, sleep disturbance, anxiety, depression, and disruption of daily activities. These psychological sequelae may lead to a lower quality of life. The desire for aesthetic beauty is increasing

*Co-first author.

†Corresponding author: CIRTECH Institute, HUTECH University (Email: ngx.hung@hutech.edu.vn).

throughout the world, especially in developing countries. Scars, particularly in areas that cannot be covered by clothing, may affect significantly the life quality of the human.



Advantage values brought from this study

- 1) Clean the wound regularly
- 2) Ensure user safety
- 3) Easy to use, easy to recycle
- 4) Low cost to support the poor

Figure 1: The wound healing process of the patient.

Of all these commonly injured parts of the human body, the head region at the head and face is the most important and dangerous. Many studies have tried to regenerate damaged structures in this part of the body to help patients recover. As analyzed before, the reconstruction of the human body parts is divided into 3 main research directions [1–3], including body reconstruction [4–6], reconstruction of the extremities [7, 8] and reconstruction of the head as shown in Fig. 3. Reconstruction of the extremities has been the subject of numerous publications, particularly with regard to the hands [9–13] and legs [14–18]. Most studies concerned on limb reconstruction due to the relative safety of these areas compared to other parts of the body. In addition, this area is easy to handle and assemble and is less dangerous for the patient. Similarly, reconstruction of the body area is divided into the reconstruction of the spine [19–25] and the rib cage [26–30]. More importantly, two main research directions concerning on the head region consists of facial reconstruction [31–33] and skull reconstruction [34, 35]. Also, injuries to the head can be particularly dangerous and may cause a higher death rate than in other areas. Therefore, research on the reconstruction of the face and skull has still been very challenging. That is a reason why studies on head injuries are also much fewer than injuries to other areas of the body.

Processes to reconstruct virtual structures in the human body are being developed quickly with the help of machine learning models. 3D prototypes for research purposes can be then created by additive manufacturing technologies or 3D printing. The use of machine learning approaches to upgrade 2D models into 3D models of the human facial area is a very potential topic that has been interested in research over the past few decades. Investigating this tough model requires both the recognition algorithm and the correctness of the product after the reconstruction model. The difficulty of the 3D structural reconstruction stems from associated concerns such as the position of facial features, the convexity of the model, and the use of multiple colors to identify the most correct 3D model. In other words, the nature of the problem is heavily influenced by the algorithm model used. Table 1 lists the key algorithms employed for the reconstruction of the face model.

As illustrated in Table 1 and Fig. 2, the relevant studies on the reconstruction of 3D human facial have been extensively devised for a long time. However, the above studies still exist the following gaps:

- The dataset of faces and facial scars is lacking due to medical research ethics. The ethical considerations in medical research aim to protect the privacy and dignity of human subjects participating in the studies. In the case of facial scars, the inclusion of images of individuals with such scars may lead to stigmatization and discrimination, particularly in employment and social settings. This potential harm to the participants' well-being may outweigh the benefits of having a comprehensive dataset for facial recognition or other related applications. As a result, the lack of a dataset of faces with facial scars may limit the accuracy and effectiveness of facial recognition technologies in identifying individuals with such scars.

Table 1: Some algorithms for the reconstruction of face used in recent years

Period	Restrictions	External links	Sources
Up to 2016	<ul style="list-style-type: none"> - Machine learning models have been widely adopted and proven to be useful in solving various features of detection problems. - Several advanced methods have been proposed in the previous states including creating 3D models from signals and recreating 3D models using RGBD scanning. In addition, some applications for recreating human faces, as well as applications that operate on human faces recreated through video. - The development during this period is mainly inhibited by the hardware limitations of devices such as smartphones and scanners. 	Artificial Neural Network	[36–39]
		Deep Learning	[40–43]
		Ensemble Methods	[44–48]
		Dimensionality Reduction	[49–52]
		Bayesian	[53–56]
		Decision Tree	[57–59]
		Regression	[60, 61]
Up to 2022	<ul style="list-style-type: none"> - New algorithms related to artificial intelligence have been extensively developed, and they are being integrated to create remarkable technological advancements. - The hardware systems, including machines that offer high accuracy, convenience, and safety for users, have been developed. - Several applications directly interact with the human body with the aid of current 3D printing technology and the development of bio and metal materials. 	Deep Learning	[12, 13, 26, 39, 41, 42, 45, 62–66]

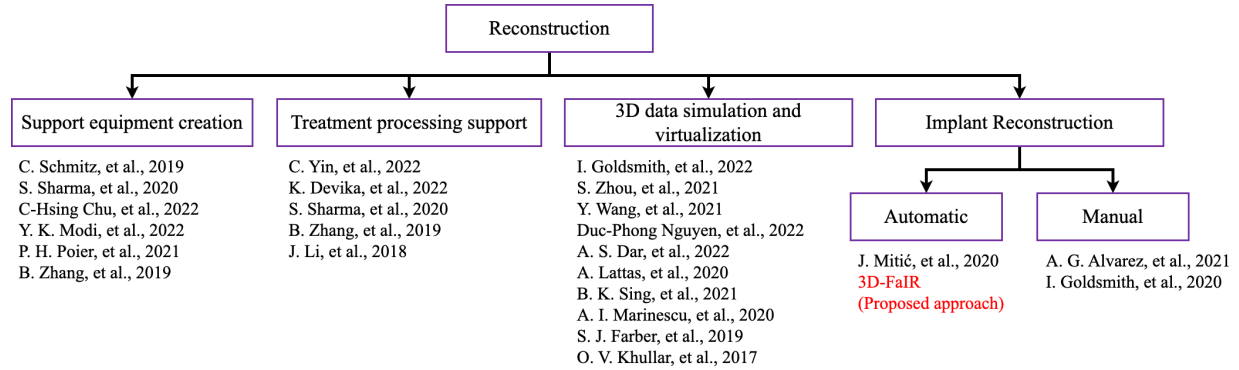


Figure 2: Some studies in the direction of 3D reconstruction.

- The facial reconstruction process is still inaccurate due to facial defects because the filling-removal process were designed manually. When addressing facial imperfections, the manual processes of filling and sculpting are typically carried out by a surgical physician. However, Such a manual approach is prone to inaccuracies and inconsistencies, which can lead to suboptimal outcomes for the patient. Additionally, the level of skill and experience of the surgeon can further impact the precision of the procedure, increasing the likelihood of errors. While technology such as computer-aided design (CAD) and 3D printing can partially address these shortcomings, they still require an expert in both the medical and technological fields. Currently, there is no automated method for generating filling material to support the surgeon in the most optimal way.
- Currently, the majority of research is centered around the manual design of 3D discrete components, with a lack of comprehensive solutions for specific body parts, especially for the facial part. At present, the bulk of research efforts in the realm of 3D design are focused on the manual creation of discrete components as nose, chin, finger joint, ankle bone, etc. Regrettably, there is a paucity of comprehensive solutions that address specific body parts, particularly the all facial region. Despite the increased utilization of 3D printing technologies in the medical field, there remains a significant gap in the development of automated methods for generating filling material that is optimized for facial imperfection correction procedures. This gap highlights a critical need for further research to develop effective techniques for automating the generation of 3D models

that accurately capture the intricacies of the facial region. Such advances would be invaluable in streamlining the surgical process, increasing accuracy, and ultimately leading to improved patient outcomes.

As a result, to compensate for the deficiencies of earlier studies on this topic, the current work suggests the use of 3D object reconstruction of the fully convolutional mesh autoencoder model in the face regeneration problem for trauma patients. The research has exploited advanced machine learning models in image processing and analysis to rebuild facial scars. Facial wound patient models, replicated in virtual space using artificial intelligence, can match true scar states and form more complicated scar models. The findings also show that the proposed method delivers a complete face reconstruction based on the remainder of the face, as opposed to reconstructing by joining one human body component to another. To optimize the present research model, we utilized an improved outlier technique to isolate patients' wounds and generate suitable wound cover models. The obtained results show the potential for developing safe and convenient products to assist patients in their recovery.

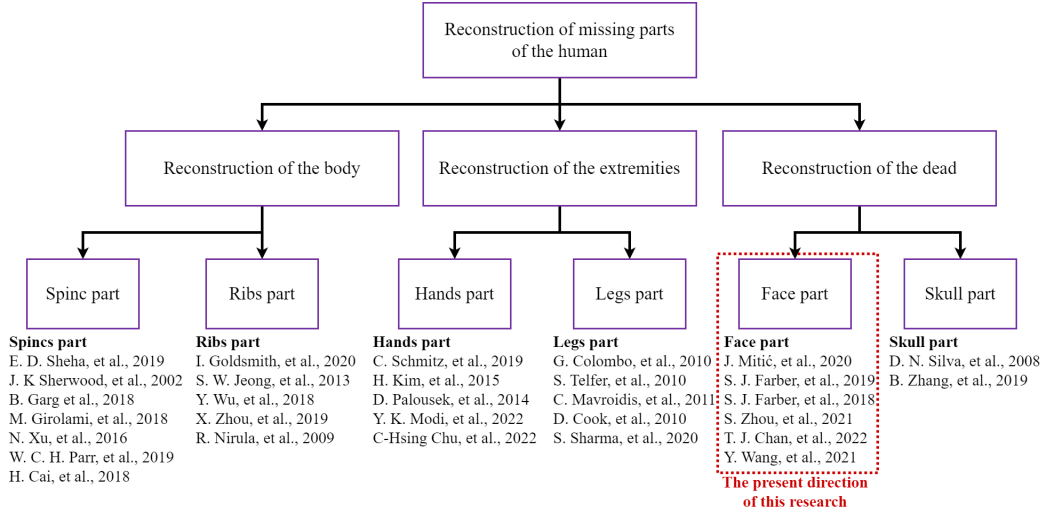


Figure 3: Some studies on restructuring the human body.

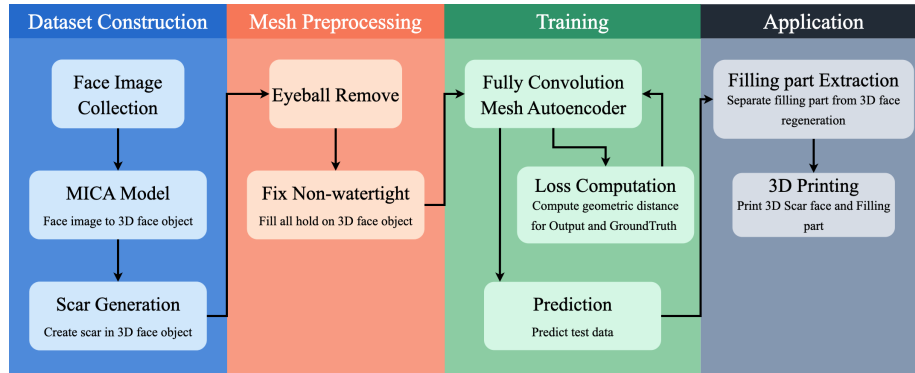


Figure 4: Overview of the data flow process for problem processing.

2 Materials and methods

In this section, we present an efficient method to create a human head mesh dataset based on the MICA model by Zielonka et al. [62]. The research direction in the field of defective faces has been severely limited due to the lack of data, mostly caused by patient privacy concerns. To address this issue, we have generated the Cir3D-FaIR dataset using the technique we called Virtual Space. This dataset not only ensures patient privacy but can also be made available publicly to support other researchers. Four main processes including dataset construction, mesh preprocessing, training, and application have been solved. As shown in Fig. 4 shows, we have started processing and building the data by collecting the data of the human face image and using the MICA model to get the original 3D face object. Scar

Generation is responsible for creating random scars for 3D face objects. Next, in the mesh preprocessing part, we have to refine the data to better fit the Fully Convolution Mesh Autoencoder model such as removing eyeballs and filling holes to fix the non-watertight error. In the Training part, we introduce a new training strategy by changing the calculation object of the loss function. Finally, in the Application part, we offer a method to bring this problem to life by extracting the fill and sending it to 3D printing for further treatment purposes.

2.1 Generation of dataset

For the first phase, we collected photographs of the faces of 3687 individuals from various nations around the world in order to assure the coverage of facial information of all races. Using the MICA model - Towards Metrical Reconstruction of Human Faces model delivers SOTA - State of the Art results on datasets converted from 2D models to 3D models [62], these 3687 photographs of human faces were converted to 3D models as displayed in Fig. 5.

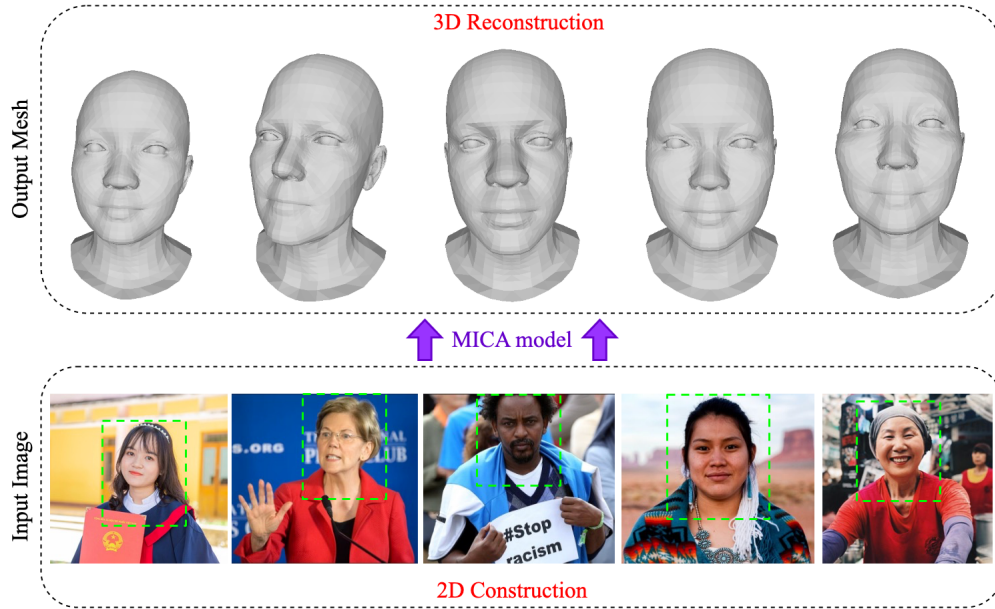


Figure 5: Some input and output of MICA model.

The MICA model is divided into 2 main parts: Identity Encoder and Geometry Decoder as shown in Fig. 6.

- **Identity Encoder:** The research adopts the work of Deng et al [63] sub-center ArcFace network in pre-trained facial recognition on large-scale 2D picture datasets. The previous research has revealed the individual characteristics of every single face which can significantly differ in expression, light, and image capability from the Glint360K dataset [67]. According to the present study, the ArcFace sub-center is constructed on the ResNet100 architecture, which is capable of being robust to photographs obtained in surroundings with low stability. Furthermore, the author has extended the architecture of Sub-center ArcFace with a mapping network, which maps the features that Sub-center ArcFace wants to be discernable by their geometry decoder. The network is made up of three fully connected linear hidden layers, and ReLU is used for activation.
- **Geometry Decoder:** Since the 3DMM model was too good for facial representation, the author focused on model-based decoder development. In this model, the author uses FLAME [68], which is a model that uses linear shape space trained from 3800 human head scans, and combines that linear shape space with jaws, necks, eyeballs, pose-dependent corrective blend shapes, and additional global expression blend shapes. In addition, the model was trained at over 33,000 scans and produced more outstanding results than models such as the Face Ware House [69] and Basel Face Model [70].

The present study gathers data after using the MICA model, and the replicable model is presented in Fig. 6. The findings acquired from Fig. 6 are per capita mesh models, and two eyeballs are isolated from the main mesh, yielding a total number of mesh points of 5023. According to the above studies, two eyeballs are not truly required in the human face restructuring model, so this research deleted two eyeballs and the recovery model produced the same findings as Fig. 7a. Because the fully convolutional mesh autoencoder model only accepts watertight mesh data [71], this research needs to

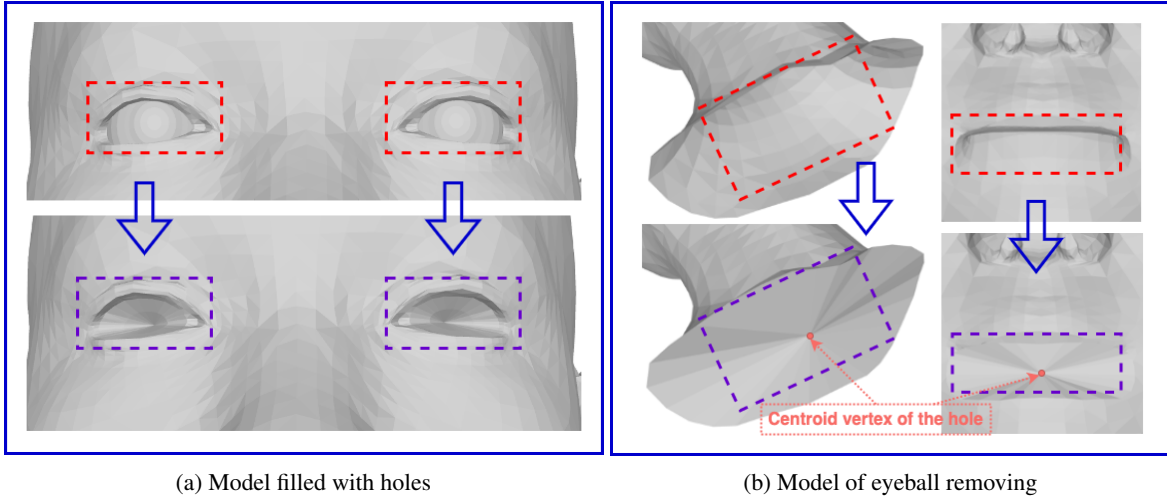
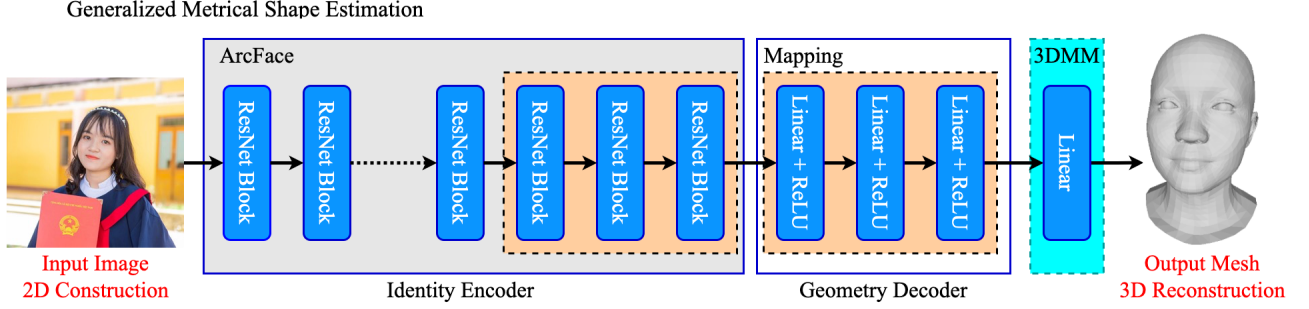


Figure 7: Geometrical figures

address the gap that is causing present mesh data to be non-watertight as Fig. 7b. The proposed method introduces a simpler and easier-to-execute strategy for filling holes in the mesh than earlier studies, including: 1) Find all the edges at the edge hole, so that all the edges in the mesh model are in one face. 2) Connect the edges with corresponding spots, forming sets of holes on the mesh. 3) Take the midway of the pore and connect all the points on the pore to that midpoint, forming a sheet pattern to cover these voids from the extracted points on the edges of the corresponding pores.

The creation of the Cir3D-FaIR dataset involves a multi-step process. First, a simulated MRI scan is created from an actual patient, with the patient's consent, and is then converted into a 3D format. Next, a large number of 3D faces are generated in Virtual Space with MICA dataset, which each product containing different errors in specific parts of the face, such as the eyes, nose, and mouth. This is done to ensure that dataset covers a wide range of possible faces. Once the 3D faces have been generated, random errors are introduced wherever possible to further increase the variability of dataset. These random errors can include anything from subtle asymmetries to more severe defects. The resulting dataset is intended to be representative of a broad range of facial defects that might be encountered in clinical practice. Throughout the process of generating the Cir3D-FaIR dataset, medical professionals are consulted to ensure that the dataset is both feasible and useful for research purposes. This includes assessing the accuracy and realism of the simulated defects, as well as evaluating the potential impact of the dataset on patient privacy. Ultimately, the goal of the Cir3D-FaIR dataset is to provide researchers with a comprehensive and privacy-protected resource for studying facial defects. By generating a diverse and realistic dataset, this research aims to enable further advancements in the diagnosis and treatment of facial abnormalities. The steps to implement in Virtual Space:

1. Choosing a focal point for facial scars;
2. Assembling the nearby locations of the scar center specified in step 1 to construct a scar region. The pattern spread out throughout the full scar region generated on the face by adjusting the height of the points in the scar area with the assumption that the scar center is the deepest spot;

3. At step 3, a concave scar region on the face with the shape, size, and depth of the scar area within a particular range is received after the reconstruction of the scar model from step 2. Random parameters, in particular, are chosen through many trials in order to achieve an empirical visual of the true structure of the actual wound that humans may encounter;
4. The investigation produces the results shown in Fig. 8 after employing the strategy presented in this work. The results revealed that while some aspects of the face are deformed, some regions on the face remain fixed and focused on the face. Although the data is not gathered directly from actual patients, we demonstrate that the proposed model is sufficient to assist the research model in simulating and solving real-world problems.

Finally, we modify the structure of the fully convolutional mesh autoencoder model by Zhou et al. [71] to train on our dataset, allowing the model to reconstruct incomplete faces.

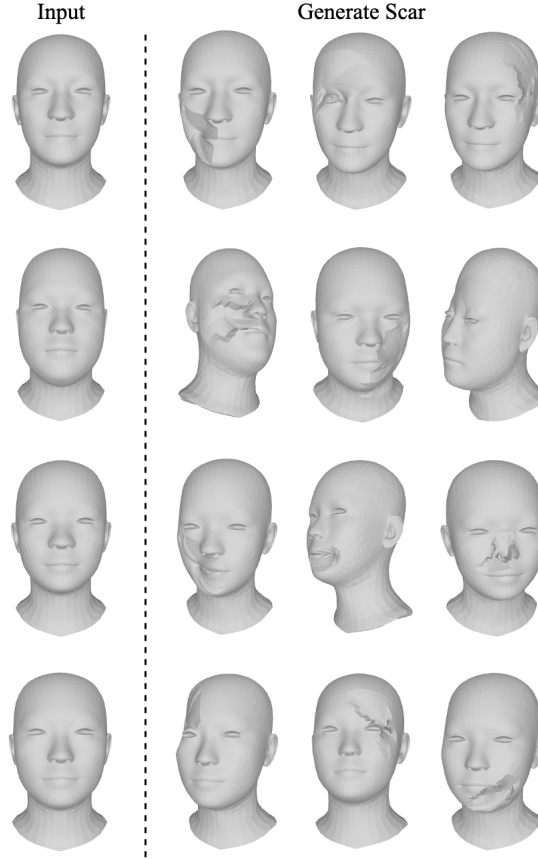


Figure 8: Some simulated models of the actual scarring process.

2.2 Fully Convolutional Mesh Autoencoder

The fully convolutional mesh autoencoder model by Zhou et al. [71] is the basis for training in this study, which aims to address the lack or limitation of using real data for ethical reasons in research. Therefore, this paper presents a new technique, that incorporates convolutional neural networks with graph models, specifically the mesh model.

2.2.1 vcConv and vcTransConv

In a regular mesh, if the topology of all neighbors is identical, the learned weight matrix determined for each neighbor vertex can be determined consistently and shared in all vertices of the grid. However, in reality, the vertices are unevenly distributed in space, and each vertex has a different connection and orientation. Therefore, we cannot directly apply the same weighting schemes. Research by Zhou et al. [71] has provided a solution to this problem by allowing the weights to vary spatially so that each vertex is free to determine its own convolution weights. At the same time, they introduced two operators, convolution and transposition, denoted *vcConv* and *vcTransConv* respectively, and called the

“coefficients of transformation” (vc) the local coefficients. These coefficients are in the range of the shared weight basis and are sampled by a set of local coefficients per neighbor. In addition, Zhou et al. [71] gave a definition of a Weight Basis (WB), which is a network formed by a virtual space of a defined size on a real-space network, where the real vertices in the mesh within the influence area of a weight basis belongs to that weight basis. The weights in WB are shared across the entire mesh, but the weights of real vertices are calculated inside that weight basis using different functions from vertex to vertex. It was shown that WB is like a pixel in a 2D CNN network, as the model directly computes on WB and then evaluates the weights back for the vertices affected by that weight basis.

Assuming that graph \mathcal{O} is the output sampled from input graph \mathcal{I} ; \mathcal{O} has N vertices and each vertex y_i is computed from a local region $\mathcal{N}(i)$ in \mathcal{I} ; $\mathcal{N}(i)$ has E_i vertices $x_{i,j}, j = 1, \dots, E_i$. Each convolution layer has one kernel basis defined as $B = \{\mathbf{B}_k\}_{k=1}^M$, where $\mathbf{B}_k \in \mathbb{R}^{I \times O}$ with local variant coefficients(vc) $A_{i,j} = \{\alpha_{i,j,k}\}_{k=1}^M, \alpha_{i,j,k} \in \mathbb{R}$. M is chosen close to the average size of a neighborhood. Then, the weight $\mathbf{W}_{i,j}$ on each edge is computed as:

$$\mathbf{W}_{i,j} = \sum_{k=1}^M \alpha_{i,j,k} \mathbf{B}_k, \quad (1)$$

and then the convolution is determined by

$$\mathbf{y}_i = \sum_{x_{i,j} \in \mathcal{N}(i)} \mathbf{W}_{i,j}^T \mathbf{x}_{i,j} + \mathbf{b}. \quad (2)$$

where $\mathbf{x}_{i,j} \in \mathbb{R}^I$ are the input feature; \mathbf{b} is the learned bias; $A_{i,j}$ are different for each vertex $x_{i,j}$ in $\mathcal{N}(i)$ of each y_i , but B is shared globally in one layer. The parameters used in this approach are learnable and shared across the entire dataset.

2.2.2 vdPool, vdUnpool, vdUpRes, and vdDownRes

To preserve the functionality of traditional Convolutional Neural Networks (CNNs), Pool and Unpool Layers are commonly used. Common types of pooling include max pooling and average pooling. Given a mesh with n vertices $V = v_1, v_2, \dots, v_n$ and their corresponding features $F = f_1, f_2, \dots, f_n$. Two pooling layers, maximum and average can be defined, respectively, as follows

$$f_{i, \text{maxpool}} = \max_{j \in \mathcal{N}(i)} f_j, \quad (3)$$

$$f_{i, \text{avgpool}} = \frac{1}{|\mathcal{N}(i)|} \sum_{j \in \mathcal{N}(i)} f_j, \quad (4)$$

where $\mathcal{N}(i)$ represents the set of neighboring vertices of vertex i in the mesh and $|\mathcal{N}(i)|$ is the number of neighboring vertices. This creates a coarser representation of the original mesh with fewer vertices, as each pooled vertex represents the average or maximum feature value of the neighborhood. The corresponding unpooling layer restores the original resolution of the mesh by copying the pooled features to their corresponding vertices. However, max or average pooling can be less effective when applied to grids with uneven peak density because they treat all regions of the input grid equally, regardless of their importance. This can result in important features being averaged out or overlooked, leading to a loss of information and a decrease in performance. To address this issue, various pooling methods have been proposed that take into account the local density of peaks or the spatial relationships between features. Thus, Zhou et al. [71] described a technique for feature aggregation using Monte Carlo sampling. The approach is inspired by the work of Hermosilla et al. [72], who estimated the vertex density using 3D coordinates of neighboring vertices. However, in more general cases, such information may not be available for each layer. In [71], instead of designing a density estimation function, the authors propose to learn the optimal variant density coefficients (vd) across all training samples. These coefficients are defined per node after pooling or unpooling, and they allow the network to adaptively adjust the density of features for each node. By learning the optimal vd coefficients, the network can better capture the important features of the input and improve performance. It is worth noting that vd is defined per node after pooling or unpooling. In [71], vdPool and vdUnpool layers act as pooling and unpooling layers in CNN, respectively. Accordingly, each local vertex j has a density coefficient is defined as follows

$$\rho'_{i,j} = \frac{|\rho_{i,j}|}{\sum_{j=1}^{E_i} |\rho_{i,j}|}, \quad (5)$$

where $\rho_{i,j} \in \mathbb{R}$ are training parameters, shared across the dataset. Specifically, Eq. (5) is an aggregate function used in vdPool and vdUnpool layers. Due to the *vd* coefficient normalization, the vdPool and vdUnpool do not perform any rescaling nor change the mean values of the input feature map. Similarly, the residual layer is written as:

$$\mathbf{y}_i = \sum_{x_{i,j} \in \mathcal{N}(i)} \rho'_{i,j} \mathbf{C} \mathbf{x}_{i,j}. \quad (6)$$

If the input and output feature dimensions are identical, then \mathbf{C} represents an identity matrix. However, if the input and output feature dimensions differ, then \mathbf{C} is a learned $O \times I$ matrix that is learned and shared across all graph nodes. According to this layer, a residual block is used for up-and-down sampling. At this point, the input is run

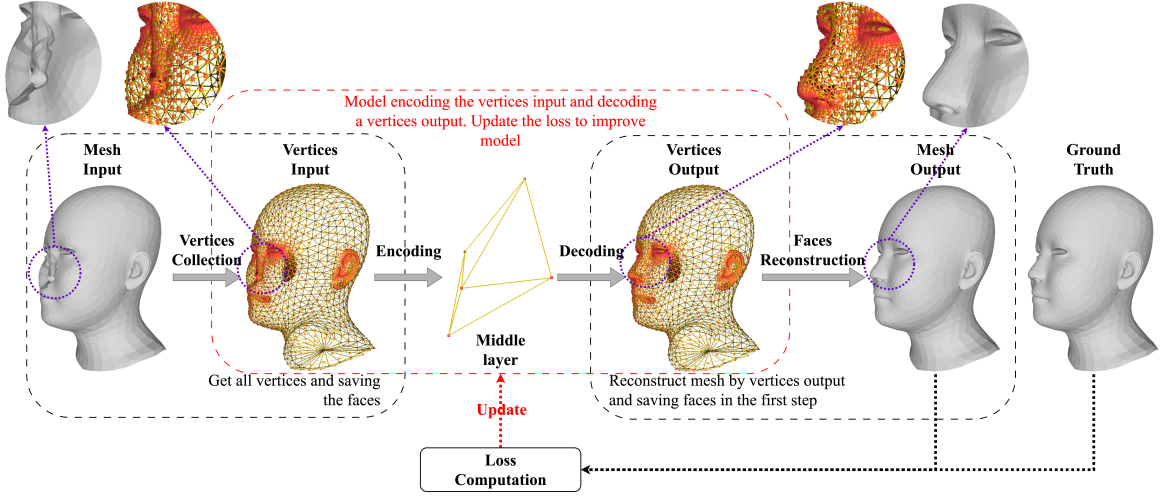


Figure 9: The coaching model we recommend.

through vcConv for down-sampling or vcTransConv for up-sampling and then the data is run through the activation layer function.

We conduct the analysis to choose the appropriate activation function for the problem. The Rectified Linear Unit (ReLU) and the Exponential Linear Unit (ELU) are both popular activation functions used in neural networks. They are both non-linear functions that introduce non-linearity into the output of a neural network, which is necessary for the network to learn complex patterns in the data. The ReLU function is defined as:

$$f(x) = \max(0, x),$$

where x is the input to the activation function. The ReLU function is a piecewise linear function that returns zero for negative inputs and the input value itself for positive inputs. The ReLU function has several advantages, including its simplicity, computational efficiency, and sparsity. The ELU function, on the other hand, is defined as:

$$f(x) = \begin{cases} x & \text{if } x > 0, \\ \alpha(\exp(x) - 1) & \text{if } x \leq 0, \end{cases} \quad (7)$$

where α is a hyperparameter that controls the value of the function for negative inputs. The ELU function is a smooth and non-monotonic function that returns the input value for positive inputs and has an exponential component for negative inputs. The ELU function has several advantages, including its smoothness, differentiability, and small negative output for negative inputs. One key advantage of the ELU function over the ReLU function is its ability to avoid the “dead ReLU” problem. In some cases, the ReLU function can cause neurons to become permanently inactive if their output falls below zero. This can lead to a reduction in the expressive power of the network and lower performance. The ELU function avoids this problem by having a non-zero output for negative inputs, which can help to prevent neurons from becoming inactive. Another advantage of the ELU function is its small negative output for negative inputs. This can help to improve the robustness of the network to noise and outliers, which is important in many applications.

From the above analysis, we can see that ELU is roughly smooth while ReLU is completely smooth. Therefore, ReLU is chosen as the activation function for this problem. The output from the ELU activation layer is combined with the output from the vdDownRes or vdUpRes layer and produces the final output. The implementation process is shown in Figure 9.

2.3 Training strategy

The selection of an appropriate loss function is essential in many machine learning problems, including mesh reconstruction. Let $v_i(x, y, z) \in \mathcal{M}_{in}(V, E, F)$ and $v'_i(x', y', z') \in \mathcal{M}_{out}(V', E', F')$ be the vertices in the input and output mesh, respectively. In [71], the loss function is calculated as the average of the sum of Euclidean distances between the corresponding vertices in the input mesh and output mesh. Accordingly, the loss function is written as follows:

$$d(v_i, v'_i) = \|v_i - v'_i\|_2. \quad (8)$$

Therefore, the loss function can be expressed as

$$\mathcal{L}(\mathcal{M}_{in}, \mathcal{M}_{out}) = \frac{1}{n} \sum_{i=1}^n d(v_i, v'_i), \quad (9)$$

where $n = n(E) = n(E')$ is the number of vertices.

Zhou et al [71] described a training model in which both the input and the comparison value are used to compute the output from the model. This approach helps the model to learn similar to the structure of the input mesh. However, our goal is to train a model to locate the wound and reconstruct it to resemble a natural face. Therefore, this loss function needs to be justified. To solve this problem, we introduce the loss function by modifying the training architecture of the fully convolutional mesh autoencoder model.

According to Subsection 2.1, we get 3687 ground truth mesh faces of people before the injury. In the problem of this research, the input and the ground truth are two different meshes. Thus, the inclusion of the input is a human head mesh with wounds and the ground truth is a human head mesh before the injury, and then the output generated from the model is calculated with that ground truth. Similar to \mathcal{M}_{in} , \mathcal{M}_{out} , let $v''_i(x'', y'', z'') \in \mathcal{M}_{gt}$ be the vertices in the ground truth mesh. Then, the loss function is adjusted as follows:

$$\mathcal{L}(\mathcal{M}_{out}, \mathcal{M}_{gt}) = \frac{1}{n} \sum_{i=1}^n d(v'_i, v''_i) = \|v'_i - v''_i\|_2, \quad (10)$$

where $d(v'_i, v''_i)$ is the Euclidean distance of the vertices on \mathcal{M}_{out} and \mathcal{M}_{gt} ; $n = n(E') = n(E'')$ is the number of vertices. With this correction, the model can learn how to repair the damage in a way that brings the injured face back to its original state, rather than simply filling the wound. The proposed training model from this research is exhibited in Fig. 9.

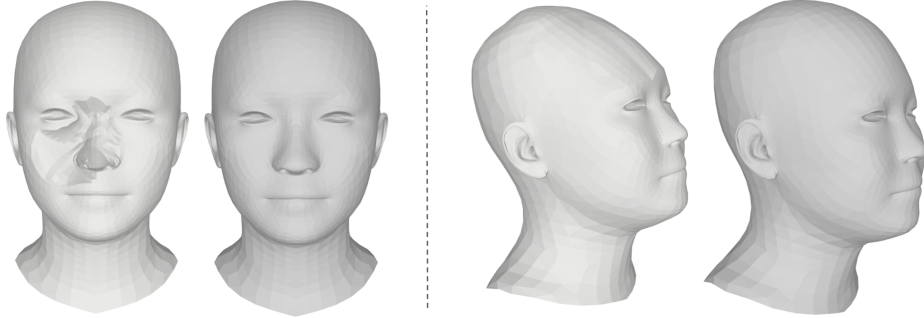


Figure 10: Results obtained from the proposed model.

2.4 Filling extraction

Fig. 10 showed results derived from the training model in Section 2.3. For the surgery of patients, the wound filling part can be then reproduced by the use of 3D printing technology. We introduce a new technique called “filling extraction” which has been implemented to fill in the missing parts with high accuracy and low computational cost. In particular, the input mesh and the ground truth mesh are both created from the same original mesh, as given in Section 2.1. The output mesh tends to reform like the ground truth mesh. Therefore, the model can take the output mesh “minus” the input mesh to obtain the filling part of the wound on the face. Because the output mesh is generated from a deep learning model, it itself exists certain errors, which need to be fixed to achieve the most accurate model. Therefore, when taking the output mesh “minus” the input mesh, in addition to filling the wound area, the wrong parts are also removed according to the concatenate mesh as illustrated in Fig. 11a. To remedy this, the outlier method was used to eliminate the underlying errors. It is noted that the fully convolutional mesh autoencoder [71] model is characterized by the fact that the output and the input have the same number of points and different point order. Accordingly, we concatenate both the input and the output in three-dimensional space. We assume that D is the set of distances of $v_i(x, y, z) \in \mathcal{M}_{in}(V, E, F)$ and $v'_i(x', y', z') \in \mathcal{M}_{out}(V', E', F')$ described by:

$$D := \{d(v_i, v'_i)\}_{i=1}^n = \{\|v_i - v'_i\|_2\}_{i=1}^n = \left\{ \sqrt{(x_i - x'_i)^2 + (y_i - y'_i)^2 + (z_i - z'_i)^2} \right\}_{i=1}^n \quad (11)$$

where n is the number of vertices of input and output meshes. We calculate the mean μ_D and variance σ_D from the set D , respectively, as follows

$$\mu_D = \frac{1}{n} \sum_{i=1}^n D_i, \quad \sigma_D = \sqrt{\frac{1}{n} \sum_{i=1}^n (D_i - \mu_D)^2}, \quad (12)$$

where n is the number of elements in the set D , and D_i is the i -element of the set D . We define the outlier extraction formula to show the error correction as follows

$$D_{outlier} := \{(v_i, v'_i) \mid |d(v_i, v'_i) - \mu_D| > 2\sigma_D\}, \quad (13)$$

where $1 < i < n$. From $D_{outlier}$, we get the coordinates of the outliers on the input mesh and output mesh respectively. The outliers are then concatenated into space, which gets the same mesh as the concatenate outlier mesh in Fig. 11. Since the concatenate outlier mesh is still two separated mesh parts, we connect them by staying at the outer edges. Then, we take additional vertices from the output mesh that are directly connected to each vertex at the outer edge of the outlier output mesh. Then, the calculation joins the outlier input mesh and the newly added vertices of the outlier output mesh together with the result eventually formed a filling mesh for the fig-like wound as shown in Fig. 11.

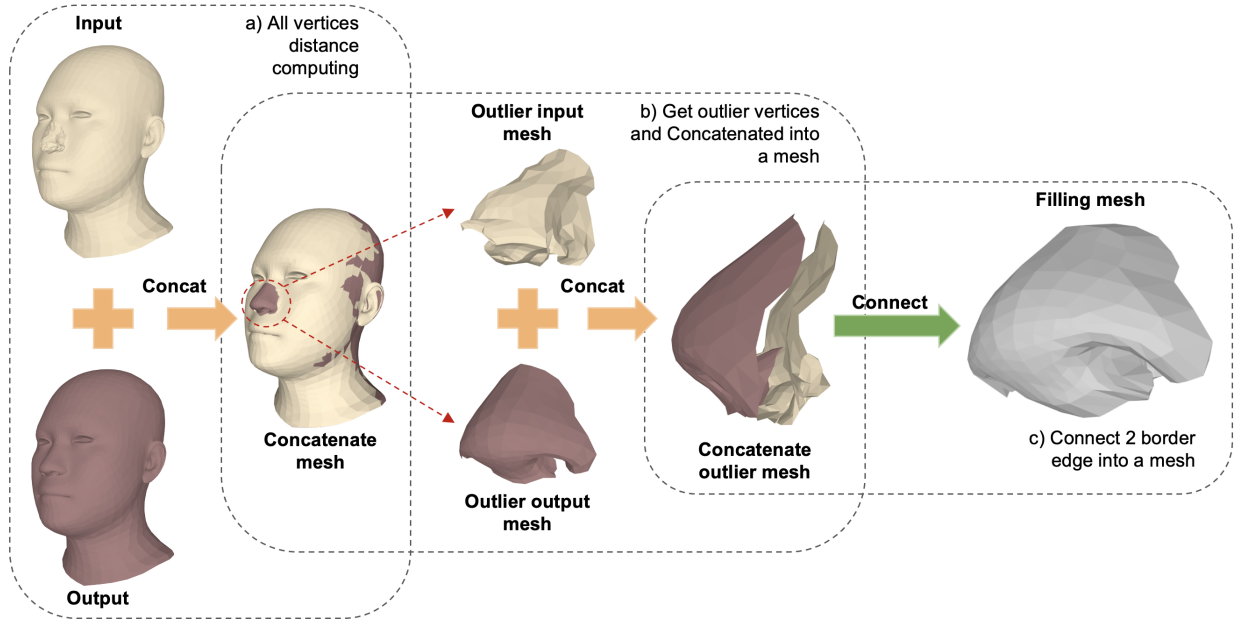


Figure 11: The procedure for the wound filling part.

3 Results and discussion

The present research reveals the results of training the model to restore the facial structure when scarred in this part. The models were trained on the 2D-manifold training set and watertight mesh of the injured skull, as described in Section 2.3. The scale used is that each human head mesh generates 10 human head meshes with wounds at random in a virtual space environment. Moreover, in the present approach, the visual model is likely to mirror the reality of individuals with facial injuries. Thus, the final dataset consists of 40458 human head mesh, including 3678 ground truth and 36780 input, derived from the starting dataset of 3687 human head mesh. As compared to previous studies, the current work consider the most hypothetical dataset of human faces available in the literature. The dataset generated by this work does not violate medical research ethics. In addition, it is also accessible to most models of injury in practice and those that are more severely harmed than they actually are. We employ 80% of the aforesaid data as a training model, 10% for validation, and the remaining 10% for testing using this enormous data set. The facial selectivity model as shown in Fig. 12 uniformly divides the points in the middle layer, allowing the model to better replicate the facial parts with the figure trained with l_1 reconstruction loss and Adam optimizer. We test the model on the test data and generate the statistics shown in Table 2, and the error used is Geometric Distance. The results show that, while the single vertex error can be as high as 4.5643, the mean error of the overall vertices of mesh is only 2.75×10^{-1} . This demonstrates the correctness of the model in the overall vertices of the mesh in the majority of circumstances. Furthermore, this study

Table 2: Statistics extracted from the test suite (3678 meshes).

Method	Error (geometric distance)	Figure reference
Min vertices distance	2.26×10^{-3}	Fig. 13a
Max vertices distance	4.564300	Fig. 13b
Mean vertices distance	2.75×10^{-1}	Fig. 13c
Min of Mean vertices distance	1.35×10^{-1}	Fig. 13d
Max of Mean vertices distance	6.64×10^{-1}	Fig. 13e

may graphically represent the results displayed in Table 2 and Fig. 15, where the chroma statistics of meshes displayed in Fig. 13 are derived based on the geometric distance of the vertices corresponding to output mesh and ground truth mesh. The research then randomly retrieved the outputs of the model on the test set, as shown in Fig. 14, to gain a better understanding of the outcomes. Simultaneously, the test employs the extraction of the filler, as shown in Fig. 16, to proceed to the 3D printing procedure for wound restoration.

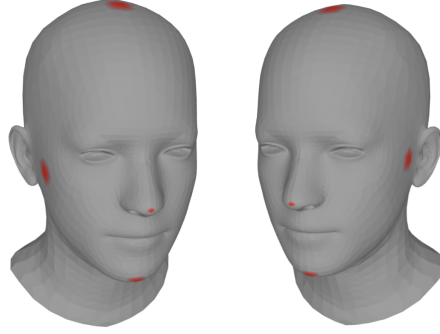


Figure 12: Illustration for the middle layer of the model.

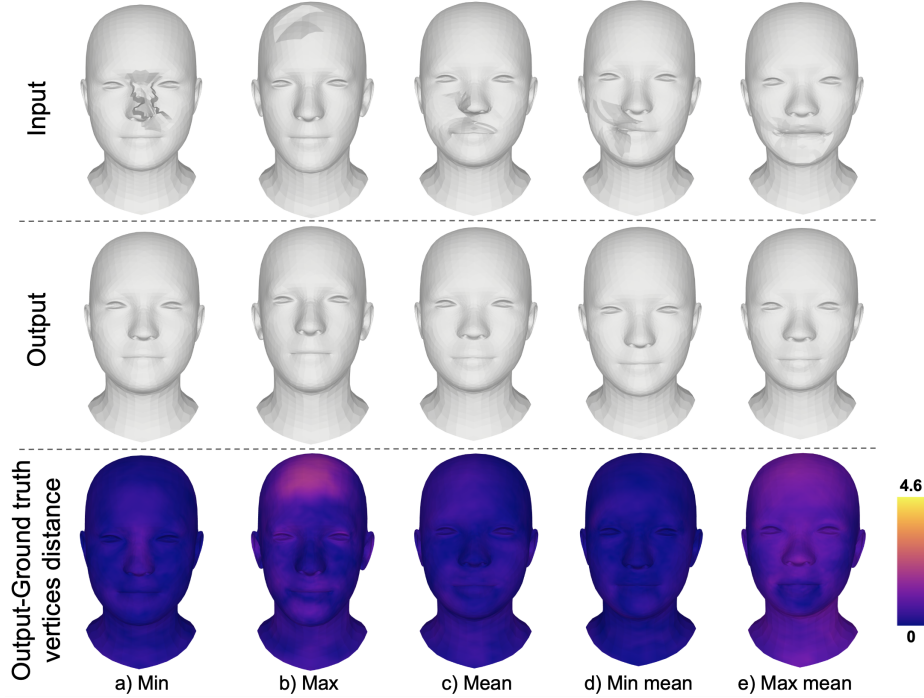


Figure 13: The results are statistically extracted from the model with the test suite (3678 meshes).

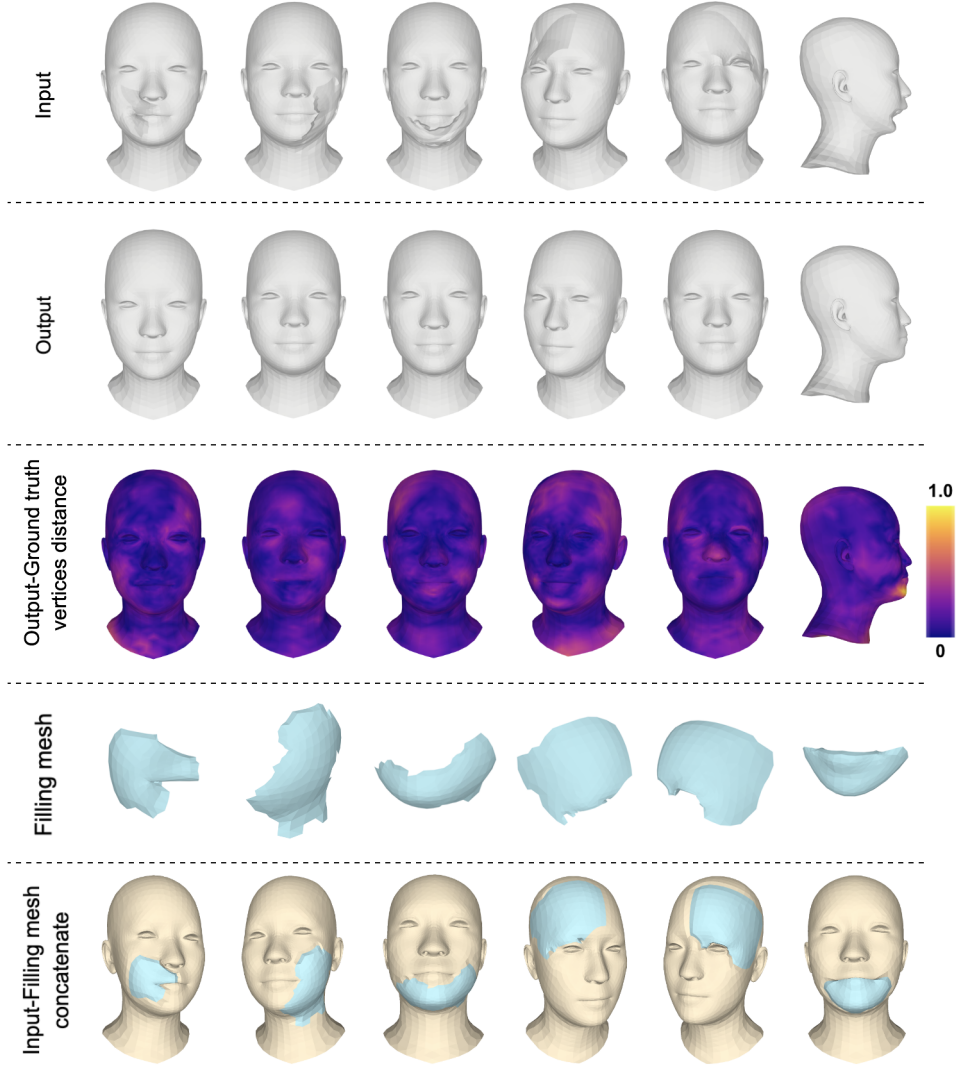


Figure 14: The results were randomly extracted from the model with the test suite (3678 meshes).

4 Conclusions

This study explored the benefits of using the fully convolutional mesh autoencoder model for 3D object regeneration of individuals with facial trauma defects. The obtained results showed the most prominent features as follows

- The virtual scar construction method allows the visual model in a virtual environment to accurately replicate the scars of patients with facial injuries. The research used a final dataset of 40,458 human head meshes, which is considered the most comprehensive human face dataset currently available. This dataset was created from an original set of 3,687 human head meshes and did not violate research ethics in medicine as it did not involve direct treatment of patients, but still provides access to a range of injury models and severe cases.
- The research results also support the proposed training method, which allows for the regeneration of facial scars based on the rest of the actual face. The model is able to accomplish this without mechanically reproducing scars or attaching one part of the person to others. The present work suggests using the outlier technique to separate the wound, which has been used to create a wound model for the entire face. The results obtained may provide useful insights for doctors during the re-surgery of patients' wounds. However, the model has limitations in its ability to accept a wide range of inputs, and future studies aim to address this issue in order to improve its practicality and overall strength.

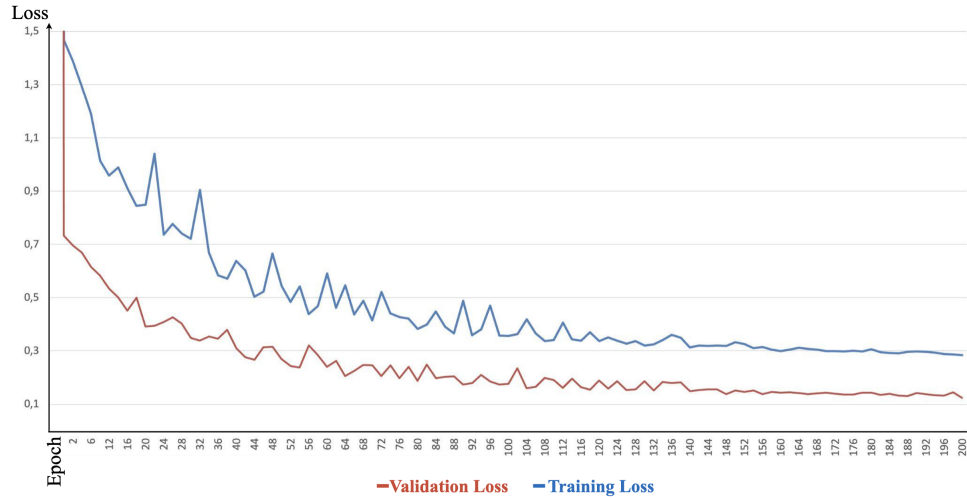


Figure 15: The loss function value corresponding to each Epoch.

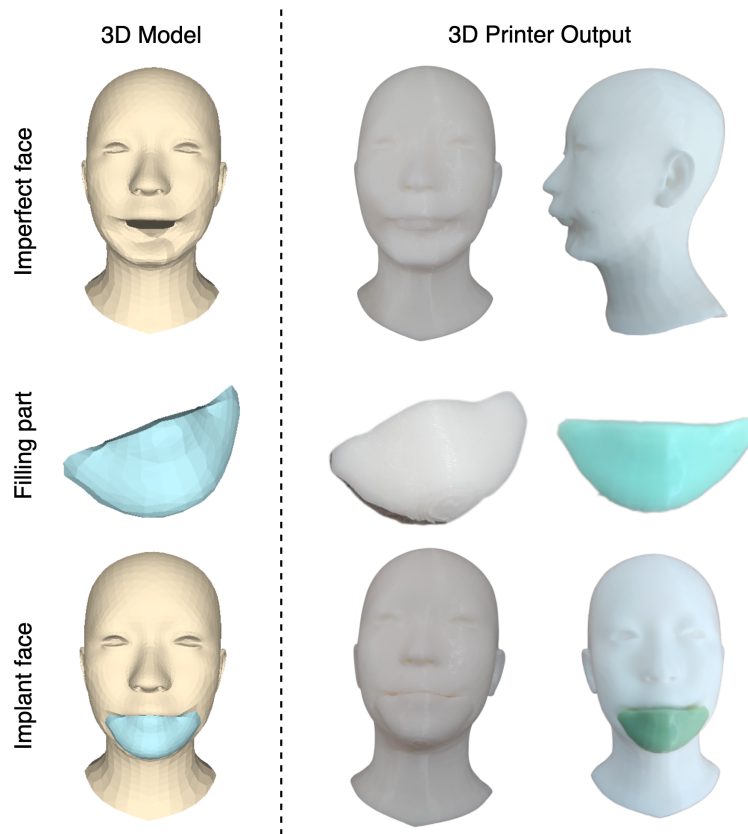


Figure 16: 3D printer output from our model result.

- The actual experiment results, as shown in Fig. 16, indicate that 3D printing technology has the potential to improve the treatment process for patients. Firstly, it supports surgeons and patients in gaining a better understanding of the final results when the treatment process is completed. Secondly, this technology replaces traditional molding methods, enabling quicker mold sample creation and assisting surgeons in adapting to each stage of patient recovery. Finally, the combination of this research with bioprinting technology has the potential to create a filling part with biological materials that are not irritating to human skin and are implanted in the face to construct a natural-looking facial structure for patients. This is a promising development, as bioprinting

technology allows for the creation of complex tissue structures that can be used for various medical applications such as drug testing, developing new therapies, and creating replacement body parts. These findings underscore the importance of ongoing research and development in the field of 3D printing technology and its potential to improve patient outcomes.

- A novel wound-covering model has been developed through this research, enabling patients to conceal facial imperfections. We hope this paper also leads to the creation of products that simplify and ensure the safe treatment of wounds during the healing process. The benefits of the current paper serve as a valuable aid for individuals suffering from illnesses in underprivileged, underdeveloped, and war-affected countries. The data generated from the present method is enriched and stored on our app system <https://ht3dprint.com>.

Acknowledgments

We would like to thank Vietnam Institute for Advanced Study in Mathematics (VIASM) for hospitality during our visit in 2023, when we started to work on this paper. It is important to highlight that the introduction of this article underwent refinement to enhance its readability, using a Large Language Model (LLM) called ChatGPT from OpenAI, based on our initial paper. Authors are accountable for the originality, validity, and integrity of the content of our submissions. The use of this AI-assisted technology is permitted by the publisher's policy.

References

- [1] M.T. Fitch, B.A. Nicks, M. Pariyadath, H.D. McGinnis, and D.E. Manthey. Basic Splinting Techniques. *The New England Journal of Medicine*, 359(26):32, 2008.
- [2] Boqing Zhang, Xuan Pei, Changchun Zhou, Yujiang Fan, Qing Jiang, Alfredo Ronca, Ugo D'Amora, Yu Chen, Huiyong Li, Yong Sun, and Xingdong Zhang. The biomimetic design and 3D printing of customized mechanical properties porous Ti6Al4V scaffold for load-bearing bone reconstruction. *Materials & Design*, 152:30–39, August 2018.
- [3] Chuan Yin, Teng Zhang, Qingguang Wei, Hong Cai, Yan Cheng, Yun Tian, Huijie Leng, Caimei Wang, Shiqing Feng, and Zhongjun Liu. Tailored surface treatment of 3D printed porous Ti6Al4V by microarc oxidation for enhanced Osseointegration via optimized bone in-growth patterns and interlocked bone/implant Interface. *Bioactive Materials*, 7:26–38, January 2022.
- [4] M.B.B.S. Ira Goldsmith, F.R.C.S.Ed MD, F.R.C.S. RCPS, and F.R.C.S. CTh. Chest Wall Reconstruction With 3D Printing: Anatomical and Functional Considerations. *Innovations: Technology and Techniques in Cardiothoracic and Vascular Surgery*, 17(3):191–200, June 2022.
- [5] Alba Gonzalez Alvarez, Peter Li Evans, Lawrence Dovgalski, and Ira Goldsmith. Design, additive manufacture and clinical application of a patient-specific titanium implant to anatomically reconstruct a large chest wall defect. *Rapid Prototyping Journal*, 27(2):304–310, January 2021.
- [6] O.V. Khullar and F.G. Fernandez. Prosthetic reconstruction of the chest wall. *Thoracic Surgery Clinics*, 27:201–208, 2017.
- [7] Paloma Hohmann Poier, Mateus Collares Weigert, Gabriel Chemin Rosenmann, Maria Gabriela Reis Carvalho, Leandra Ulbricht, and José Aguiomar Foggiatto. The development of low-cost wrist, hand, and finger orthosis for children with cerebral palsy using additive manufacturing. *José Aguiomar Foggiatto*, 73(3):445–453, 2021.
- [8] Jianyou Li and Hiroya Tanaka. Feasibility study applying a parametric model as the design generator for 3D-printed orthosis for fracture immobilization. *3D Printing in Medicine*, 4(1):1–15, 2018.
- [9] Cristiane Schmitz, Yvi Tiemi Mori, Humberto Remigio Gamba, Percy Nohama, and Mauren Abreu Souza. Development and Evaluation of a Customized Wrist-Hand Orthosis using 3D Technology for a Child with Cerebral Palsy - A Case Study. In *41st Annual International Conference of the IEEE Engineering in Medicine and Biology Society (EMBC)*, Berlin, Germany, 2019.
- [10] Huhn Kim and Seongwon Jeong. Case study: Hybrid model for the customized wrist orthosis using 3D printing. *Journal of Mechanical Science and Technology*, 29:5151–5156, 2015.
- [11] D. Palousek, J. Rosicky, D. Koutny, P. Stoklásek, and T. Navrat. Pilot study of the wrist orthosis design process. *Rapid Prototyping Journal*, 20(1):27–32, 2014.
- [12] Yashwant Kumar Modi and Navneet Khare. Patient-specific polyamide wrist splint using reverse engineering and selective laser sintering. *Materials Technology*, 37(2):71–78, 2022.

- [13] I.-Jan Wang Chih-Hsing Chu, Jing-Ru Sun, and Chien-Hsiou Liu. Customized designs of short thumb orthoses using 3D hand parametric models. *Assistive Technology*, 34(1):104–111, 2022.
- [14] Giorgio Colombo, Stefano Filippi, Caterina Rizzi, and Federico Rotini. A new design paradigm for the development of custom—fit soft sockets for lower limb prostheses. *Computers in Industry*, 61(6):513–523, August 2010.
- [15] S. Telfer and J. Woodburn. The use of 3D surface scanning for the measurement and assessment of the human foot. *Journal of Foot and Ankle Research*, 3:1–9, September 2010.
- [16] C. Mavroidis, R.G. Ranky, M.L. Sivak, B.L. Patriiti, J. DiPisa, A. Caddle, K. Gilhooly, L. Govoni, S. Sivak, M. Lancia, R. Drillio, and P. Bonato. Patient specific ankle-foot orthoses using rapid prototyping. *Journal of Neuro Engineering and Rehabilitation*, 8(1):1–11, 2011.
- [17] D. Cook, V. Gervasi, R. Rizza, S. Kamara, and X.C. Liu. Additive fabrication of custom pedorthoses for clubfoot correction. *Rapid Prototyping Journal*, 16(3):189–193, 2010.
- [18] Shubham Sharma, Jujhar Singh, Harish Kumar, Abhinav Sharma, Vivek Aggarwal, N.Jayarambabu Amoljit Singh Gill, Saraswathi Kailasa, and K.Venkateswara Rao. Utilization of rapid prototyping technology for the fabrication of an orthopedic shoe inserts for foot pain reprieve using thermo-softening viscoelastic polymers: A novel experimental approach. *Measurement and Control*, 53(3-4):519–530, 2020.
- [19] Evan D. Sheha, Sapan D. Gandhi, and Matthew W. Colman. 3D printing in spine surgery. *Annals of Translational Medicine*, 7(5):164, 2019.
- [20] Jill K. Sherwood, Susan L. Riley, Robert Palazzolo, Scott C. Brown, Donald C. Monkhouse, Matt Coates, Linda G. Griffith, Lee K. Landeen, and Anthony Ratcliffe. A three-dimensional osteochondral composite scaffold for articular cartilage repair. *Biomaterials*, 23(24):4739–4751, 2002.
- [21] B. Garg and N. Mehta. Current status of 3D printing in spine surgery. *Journal of Clinical Orthopaedics and Trauma*, 9:218–225, 2018.
- [22] Marco Girolami, Stefano Boriani, Stefano Bandiera, Giovanni Barbanti-Bródano, Riccardo Ghermandi, Silvia Terzi, Giuseppe Tedesco, Gisberto Evangelisti, Valerio Pipola, and Alessandro Gasbarrini. Biomimetic 3D-printed custom-made prosthesis for anterior column reconstruction in the thoracolumbar spine: a tailored option following en bloc resection for spinal tumors. *European Spine Journal*, 27:3073–3083, 2018.
- [23] Nanfang Xu, Feng Wei, Xiaoguang Liu, Liang Jiang, Hong Cai, Zihe Li, Miao Yu, Fengliang Wu, and Zhongjun Liu. Reconstruction of the upper cervical spine using a personalized 3D-printed vertebral body in an adolescent with Ewing Sarcoma. *Spine*, 41(1):50– 54, 2016.
- [24] William C.H. Parr, Joshua L. Burnard, Peter John Wilson, and Ralph J. Mobbs. 3D printed anatomical (bio)models in spine surgery: clinical benefits and value to health care providers. *Journal of spine surgery*, 5(4):549–560, 2019.
- [25] Hong Cai, Zhongjun Liu, Feng Wei, Miao Yu, Nanfang Xu, and Zihe Li. 3D Printing in Spine Surgery. In *Advances in Experimental Medicine and Biology*, pages 1–27. Springer, Singapore, October 2018.
- [26] Ira Goldsmith, Peter Llewelyn Evans, Heather Goodrum, James Warbrick-Smith, and Thomas Bragg. Chest wall reconstruction with an anatomically designed 3D printed titanium ribs and hemi-sternum implant. *3D printing in medicine*, 6(1):1–26, 2020.
- [27] S.W. Jeong. Conditions of rib design for polycarbonate resin with high glossy surfaces. *Journal of Mechanical Science and Technology*, 27(10):3023–3028, 2013.
- [28] Yi Wu, Na Chen, Zhou Xu, Xiaoqin Zhang, Li Liu, Chunling Wu, Shaoxiang Zhang, Yan Song, Tao Wu, Hongxiang Liu, Meng Tang, and Wei Wu. Application of 3D printing technology to thoracic wall tumor resection and thoracic wall reconstruction. *Journal of thoracic disease*, 10(12):6880–6890, 2018.
- [29] Xue-tao Zhou, Dong-sheng Zhang, Yang Yang, Guo-liang Zhang, Ze-xin Xie, Meng-hui Chen, and Zheng Liang. Analysis of the advantages of 3D printing in the surgical treatment of multiple rib fractures: 5 cases report. *Journal of Cardiothoracic Surgery*, 14(105):1–7, 2019.
- [30] Raminder Nirula, Jose J. Diaz, Jr., Donald D. Trunkey, and John C. Mayberry. Rib fracture repair: indications, technical issues, and future directions. *World Journal of Surgery*, 33:14–22, 2009.
- [31] Jelena Mitić, Nikola Vitković, Miodrag Manić, and Miroslav Trajanović. Reconstruction of the missing part in the human mandible. In *In European Conference on Computer Vision*, Cham, 2020. Springer.
- [32] Scott J. Farber, Kerry P. Latham, Rami S. Kantar, Jonathan N. Perkins, and Eduardo D. Rodriguez. Reconstructing the Face of War. *Military Medicine*, 184(7-8):236– 246, July 2019.
- [33] Scott J. Farber, Rami S. Kantar, J.Rodrigo Diaz-Siso, and Eduardo D. Rodriguez. Face Transplantation: An Update for the United States Trauma System. *Journal of Craniofacial Surgery*, 29(4):832–838, June 2018.

- [34] Daniela Nascimento Silva, Marília Gerhardt Oliveira, Eduardo Meurer, Maria Inês Meurer, Jorge Vicente Lopes Silva, and Ailton Santa-Bárbara. Dimensional error in selective laser sintering and 3D-printing of models for craniomaxillary anatomy reconstruction. *Journal of Cranio-Maxillofacial Surgery*, 36(8):443–449, 2008.
- [35] Boqing Zhang, Huan Sun, Lina Wu, Liang Ma, Fei Xing, Qingquan Kong, Yujiang Fam, Changchun Zhou, and Xingdong Zhang. 3D printing of calcium phosphate bioceramic with tailored biodegradation rate for skull bone tissue reconstruction. *Bio-Design and Manufacturing*, 2:161–171, 2019.
- [36] Mayank Agarwal, Nikunj Jain, Manish Kumar, and Himanshu Agrawal. Face recognition using eigen faces and artificial neural network. *International Journal of Computer Theory and Engineering*, 2(4):624, 2010.
- [37] Elad Richardson, Matan Sela, and Ron Kimmel. 3D face reconstruction by learning from synthetic data. In *In 2016 fourth international conference on 3D vision (3DV)*, Stanford, California, USA, 2016. IEEE.
- [38] Li Fangmin, Chen Ke, and Liu Xinhua. 3D face reconstruction based on convolutional neural network. In *In 2017 10th International Conference on Intelligent Computation Technology and Automation (ICICTA)*, Changsha, China, 2017.
- [39] You-Wei Yuan and La-Mei Yan. A neural network approach for 3-D face shape reconstruction. In *In Proceedings. International Conference on Machine Learning and Cybernetics*, Adelaide, Australia, 2002.
- [40] Pengfei Dou, Shishir K. Shah, and Ioannis A. Kakadiaris. End-to-end 3D face reconstruction with deep neural networks. In *In proceedings of the IEEE conference on computer vision and pattern recognition*, Honolulu, HI, USA, 2017.
- [41] Sahil Sharma and Vijay Kumar. 3D face reconstruction in deep learning era: A Survey. *Archives of Computational Methods in Engineering*, 29(5):3475–3507, 2022.
- [42] Duc-Phong Nguyen, Tan-Nhu Nguyen, Stéphanie Dakpé, Marie-Christine Ho Ba Tho, and Tien-Tuan Dao. Fast 3D Face Reconstruction from a Single Image Using Different Deep Learning Approaches for Facial Palsy Patients. *Bioengineering*, 9(11):619, 2022.
- [43] A.S. Dar and S. Palanivel. Real time face authentication system using stacked deep auto encoder for facial reconstruction. *International Journal of Thin Film Science and Technology*, 11(1):9, 2022.
- [44] Jae-Yong Baek, Yong-Sang Yoo, and Seung-Hwan Bae. Generative adversarial ensemble learning for face forensics. *IEEE Access*, 8:45421–45431, 2020.
- [45] Yiming Wang, Xinghui Dong, Gongfa Li, Junyu Dong, and Hui Yu. Cascade regression-based face frontalization for dynamic facial expression analysis. *Cognitive Computation*, 14:1571–1584, 2022.
- [46] Renjie Liao, Xin Tao, Ruiyu Li, Ziyang Ma, and Jiaya Jia. Video super-resolution via deep draft-ensemble learning. In *In Proceedings of the IEEE international conference on computer vision*, Cambridge, MA, USA, 2019.
- [47] Mehmet Akif Yaman, Frank Rattay, and Abdulhamit Subasi. Comparison of bagging and boosting ensemble machine learning methods for face recognition. *Procedia Computer Science*, 194:202–209, 2021.
- [48] Fan Yeping, Yang Desheng, Ma Dong, Jiao Dian, Chi Xiaojin, and Chen Mengxian. A research on face cognition method with deep ensemble learning and feedback mechanism. In *In 2019 2nd International Conference on Information Systems and Computer Aided Education (ICISCAE)*, Dalian, China, 2019.
- [49] Changshui Zhang, Jun Wang, Nanyuan Zhao, and David Zhang. Reconstruction and analysis of multi-pose face images based on nonlinear dimensionality reduction. *Pattern Recognition*, 37(2):325–336, 2004.
- [50] Wei Wang, Yan Huang, Yizhou Wang, and Liang Wang. Generalized autoencoder: A neural network framework for dimensionality reduction. In *In Proceedings of the IEEE conference on computer vision and pattern recognition workshops*, San Juan, PR, USA, 2014.
- [51] Yasi Wang, Hongxun Yao, and Sicheng Zhao. Auto-encoder based dimensionality reduction. *Neurocomputing*, 184:232–242, 2016.
- [52] Abdelghafour Abbad, Omar Elharrouss, Khalid Abbad, and Hamid Tairi. Application of MEEMD in post-processing of dimensionality reduction methods for face recognition. *IET Biometrics*, 8(1):59–68, 2019.
- [53] Alan Brunton, Jochen Lang, Eric Dubois, and Chang Shu. Wavelet model-based stereo for fast, robust face reconstruction. In *In 2011 Canadian Conference on Computer and Robot Vision*, Newfoundland Canada, 2011.
- [54] Lyndsey C. Pickup, David P. Capel, Stephen J. Roberts, and Andrew Zisserman. Bayesian methods for image super-resolution. *The Computer Journal*, 52(1):101–113, 2009.

- [55] Igor Fedorov, Ritwik Giri, Bhaskar D. Rao, and Truong Q. Nguyen. Robust Bayesian method for simultaneous block sparse signal recovery with applications to face recognition. In *In 2016 IEEE International Conference on Image Processing (ICIP)*, Phoenix, Arizona, 2016.
- [56] Peter Claes, Dirk Vandermeulen, Sven Greef, Guy Willems, John Gerald Clement, and Paul Suetens. Bayesian estimation of optimal craniofacial reconstructions. *Forensic science international*, 201:146–152, 2010.
- [57] Abubakar M. Ashir and Alaa Eleyan. Facial expression recognition based on image pyramid and single-branch decision tree. *Signal, Image and Video Processing*, 11:1017–1024, 2017.
- [58] Shaoning Pang, Daijin Kim, and Sung Yang Bang. Face membership authentication using SVM classification tree generated by membership-based LLE data partition. *IEEE transactions on Neural networks*, 16(2):436–446, 2005.
- [59] Vahid Kazemi, Cem Keskin, Jonathan Taylor, Pushmeet Kohli, and Shahram Izadi. Real-time face reconstruction from a single depth image. In *In 2014 2nd International Conference on 3D, Vision*, NW Washington, DC United States, 2014.
- [60] Aaron S. Jackson, Adrian Bulat, Vasileios Argyriou, and Georgios Tzimiropoulos. Large pose 3D face reconstruction from a single image via direct volumetric CNN regression. In *In Proceedings of the IEEE international conference on computer vision*, Cambridge, MA, USA, 2017.
- [61] Nikolai Chinaev, Alexander Chigorin, and Ivan Laptev. Mobileface: 3D face reconstruction with efficient cnn regression. In *Proceedings of the European Conference on Computer Vision (ECCV, Workshops)*, 2018. Munich.
- [62] Wojciech Zielonka, Timo Bolkart, and Justus Thies. Towards Metrical Reconstruction of Human Faces. In *Computer Vision – ECCV 2022: 17th European Conference*, Tel Aviv, Israel, October 2022.
- [63] Jiankang Deng, Jia Guo, Tongliang Liu, Mingming Gong, and Stefanos Zafeiriou. Sub-center ArcFace: Boosting Face Recognition by Large-Scale Noisy Web Faces. In *Lecture Notes in Computer Science, Springer, Cham, European Conference on Computer Vision - ECCV 2020: Computer Vision – ECCV 2020*, pages 741–757, 2020.
- [64] Yuchu Qin, Qunfen Qi, Peizhi Shi, Paul J. Scott, and Xiangqian Jiang. Automatic generation of alternative build orientations for laser powder bed fusion based on facet clustering. *Virtual and Physical Prototyping*, 15(3):307–324, 2020.
- [65] Lequn Chen, Xiling Yao, Peng Xu, Seung Ki Moon, and Guijun Bi. Rapid surface defect identification for additive manufacturing with in-situ point cloud processing and machine learning. *Virtual and Physical Prototyping*, 16(1):50–67, 2021.
- [66] Wei Long Ng, Alvin Chan, Yew Soon Ong, and Chee Kai Chua. Deep learning for fabrication and maturation of 3d bioprinted tissues and organs. *Virtual and Physical Prototyping*, 15(3):340–358, 2020.
- [67] Xiang An, Xuhan Zhu, Yuan Gao, Yang Xiao, Yongle Zhao, Ziyong Feng, Lan Wu, Bin Qin, Ming Zhang, Debing Zhang, and Ying Fu. Partial FC: Training 10 Million Identities on a Single Machine. In *2021 IEEE/CVF International Conference on Computer Vision Workshops (ICCVW)*, Montreal, BC, Canada, 2021.
- [68] T. Li, T. Bolkart, M.J. Black, H. Li, and J. Romero. Learning a model of facial shape and expression from 4D scans. *ACM Transactions on Graphics*, pages 1–17, 2017.
- [69] C. Cao, Y. Weng, S. Zhou, Y. Tong, and K. Zhou. FaceWarehouse: a 3D facial expression database for visual computing. *IEEE Trans Vis Comput Graph*, 20:413–425, 2014.
- [70] P. Paysan, R. Knothe, B. Amberg, S. Romdhani, and T. Vetter. A 3D Face Model for Pose and Illumination Invariant Face Recognition. In *2009 Sixth IEEE International Conference on Advanced Video and Signal Based Surveillance*, 2009.
- [71] Yi Zhou, Chenglei Wu, Zimo Li, Chen Cao, Yuting Ye, Jason Saragih, Hao Li, and Yaser Sheikh. Fully convolutional mesh autoencoder using efficient spatially varying kernels. In *Proceedings of the 34th International Conference on Neural Information Processing Systems, NIPS’20*, pages 9251–9262, Red Hook, NY, USA, December 2020. Curran Associates Inc.
- [72] Pedro Hermosilla, Tobias Ritschel, Pere-Pau Vázquez, Àlvar Vinacua, and Timo Ropinski. Monte carlo convolution for learning on non-uniformly sampled point clouds. *ACM Trans. Graph.*, 37(6), dec 2018.